NeuroImage 207 (2020) 116353

Contents lists available at ScienceDirect

NeuroImage

journal homepage: www.elsevier.com/locate/neuroimage

Pypreclin: An automatic pipeline for macaque functional MRI preprocessing

Jordy Tasserie [a,b,c,1], Antoine Grigis [a,d,1], Lynn Uhrig [a,b], Morgan Dupont [a,b], Alexis Amadon [a,e], Béchir Jarraya [a,b,f,g,*]

[a] Commissariat à l'Énergie Atomique et aux Énergies Alternatives, Direction de la Recherche Fondamentale, NeuroSpin Center, Gif-sur-Yvette, France
[b] Cognitive Neuroimaging Unit, Institut National de la Santé et de la Recherche Médicale U992, Gif-sur-Yvette, France
[c] Université Paris Sud, Université Paris-Saclay, Orsay, France
[d] Analysis and Information Treatment Unit, Commissariat à l'Énergie Atomique et aux Énergies Alternatives, Gif-sur-Yvette, France
[e] Magnetic Resonance Imaging and Spectroscopy Unit, Commissariat à l'Énergie Atomique et aux Énergies Alternatives, Gif-sur-Yvette, France
[f] Neurosurgery Department, Foch Hospital, Suresnes, France
[g] University of Versailles Saint-Quentin-en-Yvelines, Université Paris-Saclay, Versailles, France

ARTICLE INFO

Keywords:
Preprocessing
fMRI
Macaque
Non-human primate
Automatic
Movement artifact
Motion artifact

ABSTRACT

Non-human primate functional MRI (fMRI) is a growing field in neuroscience. However, there is no standardized method for monkey fMRI data analysis, specifically for data preprocessing. The preprocessing of monkey fMRI data is challenged by several technical and experimental specificities of the monkey research such as artifacts related to body movements or to intracranial leads. Here we propose to address these challenges by developing a new versatile pipeline for macaque fMRI preprocessing. We developed a Python module, *Pypreclin*, to process raw images using state of the art algorithms embedded in a fully automatic pipeline. To evaluate its robustness, we applied *Pypreclin* to fMRI data acquired at 3T in both awake and anesthetized macaques, with or without iron oxide contrast agent, using single loop or multichannel phased-array coils, combined or not with intracranial implanted electrodes. We performed both resting-state and auditory evoked fMRI and compared the results of *Pypreclin* to a previously employed preprocessing pipeline. *Pypreclin* successfully achieved the registration of the fMRI data to the macaque brain template in all the experimental conditions. Moreover, *Pypreclin* enables more accurate locations of auditory evoked activations in relation to the gray matter at corrected level in the awake fMRI condition. Finally, using the Primate neuroimaging Data-Exchange open access platform, we could further validate *Pypreclin* for monkey fMRI images that were acquired at ultra-high fields, from other institutions and using different protocols. *Pypreclin* is a validated preprocessing tool that adapts to diverse experimental and technical situations of monkey fMRI. *Pypreclin* code is available on open source data sharing platform.

1. Introduction

We are witnessing an important breakthrough in the development of multimodal and multi-scale neuroimaging technologies in non-human primates (NHPs). Specifically, macaque functional MRI (fMRI) is a growing area of research over the last 20 years (Logothetis et al. 1999, 2001; Vanduffel et al., 2001; Milham et al., 2018). Monkey fMRI offers a unique opportunity to achieve inter-species comparisons, to bridge the gap between human and macaque brain recordings (Orban et al., 2004), and to dissect the very mechanisms underlying the fMRI signal both in response to sensory stimuli (Logothetis et al., 2001) and during spontaneous fluctuations (Shmuel and Leopold, 2008). Importantly, monkey fMRI can be combined with invasive experimental conditions that are hardly achievable in the clinical situation, such as general anesthesia (Barttfeld et al., 2015; Uhrig et al. 2016, 2018), intracranial electrical microstimulation (Tolias et al., 2005; Ekstrom et al., 2008), deep brain stimulation (DBS) (Min et al., 2014) or the use of preclinical contrast agents (e.g. ultra-small particles loaded with iron oxide such as monocrystalline iron oxide nanoparticle, MION) (Vanduffel et al., 2001). Finally, monkey fMRI data sharing initiatives have been recently introduced to develop open resources for non-human primate imaging (Milham et al., 2018). However, there are currently no fully validated and automated methods for macaque fMRI data analysis, specifically for the raw data preprocessing.

* Corresponding author. Neurospin imaging center, Inserm, CEA Saclay, Bat 145, 91191, Gif-sur-Yvette, France.
E-mail address: bechir.jarraya@cea.fr (B. Jarraya).
[1] these authors equally contributed to the study.

https://doi.org/10.1016/j.neuroimage.2019.116353
Received 18 September 2019; Received in revised form 8 November 2019; Accepted 10 November 2019
Available online 16 November 2019

Before any statistical analysis, preprocessing aims at cleaning and normalizing fMRI data. There are several sources of noise within the fMRI signal (Keliris et al., 2007; Pfeuffer et al., 2007). Neuronal effects on the BOLD fMRI time series coexist with non-neuronal effects such as head and/or body movements, physiological changes (e.g. cardiac and respiratory fluctuations) and MRI scanner hardware instabilities (Hagberg et al., 2008; Murphy et al., 2013). To detect task evoked fMRI responses or characterize spontaneous fluctuations in fMRI signals, the raw data from the MRI scanner require preprocessing steps. Preprocessing aims at cleaning the sources of noise within the fMRI signal to reduce eventually detection of false positive errors (Murphy et al., 2013; Caballero-Gaudes and Reynolds, 2017). Preprocessing steps generally include slice-timing correction, motion correction, coregistration, spatial normalization and smoothing. In the case of awake monkeys, they are generally head fixed, however the body movements and the chewing activity (reward intake) generate transient inhomogeneities within the magnetic field and lead to distortions within the acquired images (Keliris et al., 2007; Chen et al., 2012).

Here, we aimed at developing a robust, automatic and versatile preprocessing pipeline for macaque fMRI data to address the specific challenges of the non-human primate imaging in different experimental conditions to preprocess data that are acquired from awake or anesthetized macaques (*Macaca mulatta and fascicularis*), with BOLD or MION fMRI signal, at different magnetic fields (1.5–7T) using different coils (single loop, multichannel phased-array coils, clinical coils), combined or not with intracranial implanted electrodes.

2. Materials and methods

In this study we first developed *Pypreclin* using monkey fMRI data from our institution ('Neurospin dataset'), then tested the robustness of *Pypreclin* using monkey fMRI data from several external institutions that is made available on the Primate neuroimaging Data-Exchange platform ('PRIME-DE dataset').

2.1. Animals for the Neurospin dataset

Nine rhesus macaques (*Macaca mulatta),* five males (monkeys B, J, N, T and Y) and four females (monkeys Ji, K, R and S) were included. Animals were 3 to 14 years old and weighed between 4 and 10 kg. Monkeys B, J, Y and K were scanned in the awake condition, whereas monkeys N, T, Ji, K, R and S were scanned under anesthesia (Tables S1–S3). All procedures were conducted in accordance with the European convention for animal care (86-406) and the National Institutes of Health's Guide for the Care and Use of Laboratory Animals. Animal studies were approved by the institutional Ethical Committee (CETEA protocols #10-003, #12-086 and #16-040).

Monkeys were host individually or by group with a 12:12h light-dark cycle and radio listening on daytime. During the awake sessions, monkeys had water delivered during the training and fMRI sessions (Uhrig et al., 2014; Wang et al., 2015). For anesthesia experiments, animals fasted for at least 6 h before anesthesia induction (Uhrig et al., 2016).

2.2. fMRI data acquisition for the Neurospin dataset

2.2.1. MRI scanner and sequences

Monkeys were scanned on a 3T horizontal scanner (Siemens Tim Trio, then Prisma Fit, Erlanger, Germany) with either a single loop circular mono-channel coil (1 transmission loop and 1 channel in reception, 1Tx-1Rx, NeuroSpin, France) or a multi-channel phased-array coil (1 transmission loop and 8 channels in reception, 1Tx-8Rx, KU Leuven, Belgium) customized for monkeys. Before each task-evoked fMRI session, a contrast agent, monocrystaline iron oxide nanoparticle (MION, Feraheme, AMAG Pharmaceuticals, MA; 10 mg/kg in i.v) was injected into the monkey's saphenous vein (Leite et al., 2002; Vanduffel et al., 2001). Resting-state data were acquired either following MION injection or as BOLD fMRI. Each functional scan consisted of gradient-echoplanar whole-brain imaging. The parameters of the fMRI sequences were as follows: 1) For mono-channel coil (1Tx-1Rx) experiments: repetition time of TR = 2400 ms, echo time TE = 20.00 ms, resolution 1.50 mm^3 voxel size, 111 brain volumes per run, MION signal (Uhrig et al., 2014; Uhrig et al., 2016); 2) For multi-channel coil (1Tx-8Rx) experiments there were three distinct protocols: (i) TR = 1250 ms, TE = 14.20 ms, resolution 1.25 mm^3 voxel size, 325 or 500 brain volumes per run, BOLD signal; (ii) TR = 2400 ms, TE = 19.40 ms, resolution 1.00 mm^3 voxel size, 111 brain volumes per run, MION signal; (iii) TR = 1080 ms, TE = 13.80 ms, resolution 1.50 mm^3 voxel size, 275 brain volumes per run, MION signal (Tables S1–S3).

Anatomical scans (MPRAGE, T1 weighted, TR = 2200 ms and TI = 900 ms, resolution 0.80 mm isotropic, sagittal orientation) were performed for all macaques in order to exploit high-resolution structural images during the preprocessing step.

2.2.2. Experimental conditions

We acquired functional images in four experimental conditions: (i) BOLD fMRI or MION fMRI; (ii) using a single loop circular mono-channel coil (1Tx-1Rx, abbreviated as *Mono coil* in the figures) or a multi-channel phased-array coil (1Tx-8Rx coil, abbreviated as *Multi coil* in the figures); (iii) with or without an intracranial implanted electrode; (iv) in the awake state or under anesthesia. Over the 16 theoretical combinations (four conditions with two possibilities each, 2^4), we acquired fMRI data in 9 different combinations (Tables S1–S3).

2.2.3. Awake protocol

We acquired fMRI in awake behaving macaques as previously described (Uhrig et al., 2014; Wang et al., 2015). Animals sat in sphinx position with their head fixed in a primate chair and had to fixate a red dot (0.35 × 0.35°) within a 2 × 2° window. The eye position was monitored at 120 Hz (Iscan, Inc., MA, USA). Monkeys were rewarded with fluids throughout the acquisition based on their performance as measured by fixation rate. Only runs with a fixation rate higher than a behavioral threshold were considered for the data analysis. In the previous studies, the behavioral threshold was set at 85% (Uhrig et al., 2014; Wang et al., 2015) while in the current study we included runs with a behavioral mean threshold at 80% (Fig. 5 and S4 to S6).

2.2.4. Anesthesia protocol

We acquired fMRI in anesthetized macaques as previously described (Barttfeld et al., 2015; Uhrig et al. 2016, 2018). For the task-evoked fMRI data (Fig. 5 and S7 to S9), we scanned monkeys under propofol. Two monkeys (Monkey K, Monkey R) were trained for intravenous (i.v.) injections in the awake state. To induce anesthesia, monkeys received a bolus injection of propofol (5–7.5 mg/kg i.v.; Fresenius Kabi, France) in the saphenous vein. The anesthesia was maintained with a target-controlled infusion of propofol (Alaris PK Syringe pump, CareFusion, CA, USA) based on the 'Paedfusor' pharmacokinetic model (Absalom and Kenny, 2005; Barttfeld et al., 2015; Uhrig et al., 2016) (3.7–6.5 μg/ml). To avoid artifacts related to potential movements during MRI acquisition, we administered a muscle-blocking agent (cisatracrium, 0.15 mg/kg bolus i.v. followed by continuous i.v. infusion at a rate of 0.18 mg/kg/h, GlaxoSmithKline, France).

For the resting-state fMRI, anesthesia was induced with ketamine and dexmedetomidine (10 mg/kg + 20 μg/kg i.m. respectively) and maintained with a target-controlled infusion of propofol. Monkeys were intubated and mechanically ventilated (Aestiva/5 MRI, General Electrics Healthcare, USA). The physiology parameters were monitored during fMRI acquisitions.

2.3. Experimental design for the Neurospin dataset

2.3.1. Resting-state functional MRI (rfMRI)

We acquired resting-state fMRI (BOLD or MION) in 9 macaques with a

total of 18 runs across 14 different sessions as follows: monkey K, 3 runs (500 and 111 TR of 2400 ms); monkey S, 1 run (10 TR of 2400 ms); monkey Ji, 2 runs (500 TR of 2400 ms and 1250 ms); monkey R, 3 runs (111 TR of 2400 ms); monkey Y, 1 run (275 TR of 1080 ms); monkey J, 3 runs (500 TR of 1250 ms and 10 TR of 1080 ms); monkey B, 1 run (10 TR of 2000 ms); monkey T, 2 runs (111 and 10 TR of 2400 ms) and monkey N, 2 runs (500 and 10 TR of 1250 ms) (Tables S1–S3).

2.3.2. *Task-evoked functional MRI (tfMRI)*

A passive auditory task was designed using 3 different conditions (habituation of either low or high frequency sound trials, rare or frequent low or high frequency sound trials). Auditory stimuli were created with 'Audacity software' (version 2.0.3 for Mac OS X, http://audacity.sourceforge.net). Stimuli had two different pass-bands, 0.5–1 kHz for the low frequency sound trials (total duration of 650 ms) and 8–16 kHz for the high frequency sound trials (total duration of 650 ms), with a sinusoidal envelope. The trials of sounds were separated by a 850 ms inter-stimulus interval for a total trial duration of 1500 ms. The auditory paradigm was presented with first a rest period (14.4 s, 6 TRs) followed by 5 series of 24 sound trials (36 s, 15 TRs) each followed by a rest period (14.4 s, 6 TRs). Each 24 trials-series comprises 20 'frequent' trials (either low or high frequent sound trials) and 4 'rare' trials (either low or high frequent sound trials), to avoid saturation of the auditory cortex to either high or low frequencies. The total duration of one run was 266.4 s (111 TRs). Auditory stimuli were presented with the E-prime software (E-Studio 1.0, Psychology Software Tools) and MR-compatible headphones (MR Confon, Germany), at a level of 80 dB.

In total, we included 3 animals (monkey J, K and R) in this experiment. Functional images were acquired as MION fMRI, using a single loop 1Tx-1Rx coil (TR = 2400 ms, TE = 20 ms, resolution 1.50 mm isotropic). Data were acquired in awake macaques (52 runs during 3 sessions: monkey J, 24 runs; monkey K, 28 runs) or under anesthesia (76 runs during 3 sessions: monkey K, 32 runs; monkey R, 44 runs) (Tables S1–S3).

2.4. *Pypreclin fMRI preprocessing*

We referred as '*Pypreclin*' for the new 'Python preclinical' pipeline for monkey fMRI preprocessing. We developed the *Pypreclin* Python module to process raw images using state of the art algorithms embedded in a fully automatic pipeline. This pipeline aimed at addressing several specificities of monkey research including artifacts related to body movements, the presence of extra cranial tissues, and/or obstacles induced by factors such as intracranial implanted electrodes. This pipeline is made of the following 10 sequential steps (Tables 1 and 2).

Slice-timing: the slices of one functional volume are acquired at different time points throughout the TR. By applying the slice-timing correction, this shift is compensated allowing the whole brain signal to be assigned to a single time point of the fMRI time series. In our multi-shot Echo Planar Imaging (EPI), slice timing was performed with FSL slice timer function (FMRIB's Software Library – FSL, Oxford, U.K) (Smith et al., 2004). The actual sequence parameters were selected (e.g. TR = 2400 ms, non-interleaved, increasing order).

B_0 inhomogeneities correction: during functional acquisitions, tissue interfaces in the brain cause static field inhomogeneities, which can lead to signal distortion (Orban et al., 2003; Pfeuffer et al., 2007). The geometric distortions can be corrected by estimating a deformation field restricted to the phase-encoding direction between the anatomical and the functional data. In the context of non-human primate imaging, functional data generally display low contrast making this step unstable, and sometimes invalid (nonetheless, *Pypreclin* proposes a routine to perform such a correction). Rather than correcting the constant part of the B_0 inhomogeneities, we focused on the motion induced, time dependent distortions. This correction is performed with the SyN function of ANTS (Advanced Normalization Tool – ANTS), and has been proven particularly useful in the awake condition where we expect greater distortions due to the macaque's body movements. By default, we chose the 8th volumes, generally corresponding of 10–20 s after the start of the acquisition, in order to ensure that the macaque was fixating well and calm. In the case of reversed phase-encoded EPI sequences, which implies that the same field leads to distortion in opposite directions during both acquisitions, the correction can be performed with FSL topup. With an available field map, the unwarping of the EPI image can be directly computed with FSL FUGUE.

Reorientation: it is crucial to accurately report the exact spatial orientation of the monkey's brain (antero-posterior, right-left, cranio-

Table 1
NeuroSpin Monkey (NSM) and *Pypreclin* preprocessing steps. Main differences are highlighted with bold characters or hatched boxes.

	NSM preprocessing	Pypreclin pipeline
Slice timing	slicetimer (FSL)	slicetimer (FSL)
Motion-induced susceptibility distorsions correction	**ImageRegistrationMethod (ITK) - rigid 2D**	**SyN (ANTs) - PA restricted**
Motion correction	mcflirt (FSL)	mcflirt (FSL)
Reorientation	**reorient (NSM)**	**reorient2std (Pypreclin)**
B1 field bias correction		**N4 (ANTS)**
Masking	**bet2 (FSL)**	
Normalization		**align (JIP) - NL with mask propagation)**
Coregistration	**flirt (FSL) - affine**	**align (JIP) - rigid**
Smoothing	**gaussian_filter (scipy)**	**smooth (FSL)**
Fully automatic	Yes	Yes - with possibility of manual initialization
QC report		**Yes**

Table 2
Main preprocessing functions included in the *Pypreclin* pipeline and alternatives software. Catalog of different tools available for fMRI preprocessing and their potential specificities for macaque (bold characters). *Pypreclin* pipeline accepts random or organized structures like *BIDS* (Brain Imaging Data Structure) format, reads acquisition parameter files and can be run fully automatically (with no manual intervention).

	Included in *Pypreclin*	Alternatives (not included in *Pypreclin*)
Slice-timing correction	slicetimer (FSL)	slice_timing (SPM), 3dTshift (AFNI), interp_4dfp (4dfp)
Susceptibility distorsions correction	topup - FUGUE (FSL)	3dqwarp (AFNI), FieldMap - HySCO (SPM), N3 (MINC)
Motion-induced susceptibility distorsions correction	SyN (ANTs)	ImageRegistrationMethod (ITK), **align (JIP)**, FLIRT (FSL)
Motion correction	MCFLIRT (FSL)	3dvolreg (AFNI), realign (SPM), BrainRegistration (ANTs), cross_realign (4dfp)
Reorientation	in house implementation & reorient2std (FSL)	3dresample (AFNI), reorient (SPM), reorient_image (ANTs)
B1 field bias correction	N4 (ANTs)	3duniformize (AFNI), mri_normalize (Freesurfer), FAST (FSL), BFC (Brainsuite), segment (SPM)
Masking	**align (JIP)** & in house implementation (mask propagation)	BrainExtraction (ANTs), **3dSkullstrip (AFNI)**, bet2 (FSL), BEaST (MINC), MRTOOL (SPM)
Normalization	**align (JIP)**	Registration (ANTs), FNIRT (FSL), Normalize (SPM), **monkey_mritotal (MINC)**, volume_registration (Brainsuite), auto_tlrc (AFNI)
Coregistration	**align (JIP)**	Registration (ANTs), FLIRT (FSL), Coregister (SPM), 3dvolreg (AFNI), monkey_best_lin_reg (MINC)
Smoothing	smooth (FSL)	smooth (SPM), Registration (ANTs), 3dBlurToFWHM (AFNI)
Allow manual intervention	**align (JIP)**	
QC report	in house implementation	QAP, CheckReg (SPM), mriqc (CRN), afni_proc (AFNI)

caudal) and match it to the defined atlas landmarks. This orientation depends on the monkey position during acquisition (e.g. sphinx position, head first etc) (Vanduffel et al., 2001). *Pypreclin* takes this acquisition position into account and eventually reorients images to match the selected template's space orientation Right Antero Superior (RAS) (Vanduffel et al., 2001).

Realignment: we used a motion correction based on FSL MCFLIRT function (FMRIB's Software Library – FSL, Oxford, U.K) (Smith et al., 2004). We considered the image acquired in the middle of the run as baseline to align the other functional images of the same run.

Normalization and masking: in the context of monkey normalization, potential cofounders include the extra cranial tissues (such as chewing muscles) and intracranial implanted devices (such as electrodes) that can disrupt the optimization, thus leading to misaligned images (Keliris et al., 2007; In et al., 2017). To overcome this issue, we use the Joe's Image Program (JIP) -align routine (http://www.nmr.mgh.harvard.edu/~jbm/jip/, Joe Mandeville, Massachusetts General Hospital, Harvard University, MA, USA). This algorithm ignores these muscle tissues by projecting the mask of the template (which only needs to be defined once) back to the monkey's anatomical space. This process sometimes requires first to achieve a rough initial alignment before automated alignment. The optimization algorithm is driven by the mutual information (MI) cost function (Evans, 2008). The normalization step aligns (affine) and warps (non-linear alignment using distortion field) the anatomical data into a generic template space.

B_1 field correction: low frequency intensity nonuniformities present in the data, also known as bias field, are potential confounding in various analytical tasks, especially during alignment (Marques et al., 2010). This artifact can be corrected by multiple softwares (FSL, ANTS, Nipy, BrainVisa), and we selected the ANTS N4 normalization.

Coregistration: coregistration refers to the spatial alignment of the functional and the anatomical images. We applied a rigid transformation using JIP align (http://www.nmr.mgh.harvard.edu/~jbm/jip/, Joe Mandeville, Massachusetts General Hospital, Harvard University, MA, USA) to register the mean functional image (moving image) to the anatomical image (fixed image). To obtain the anatomical brain mask, we warped the template brain mask using the deformation field previously computed during the normalization step. Finally, by composing the normalization and coregistration spatial transformations, we aligned the functional images with the template space. The template brain mask is also warped in the native functional space in order to remove unwanted signals in the time-series (Fischmeister et al., 2013).

Time series denoising: for the denoising of resting state fMRI data, we recommend using the non-human primate adapted ICA-FIX command (https://github.com/Washington-University/NHPPipelines) for spatial Independent Component Analysis (ICA, i.e. melodic) followed by the automatic classification of components into 'signal' and 'noise' (Autio et al., 2019).

Smoothing: smoothing is generally used in fMRI analysis to improve the signal to noise ratio (SNR) (Caballero-Gaudes and Reynolds, 2017; Scouten et al., 2006) and to compensate for remaining variability between individuals during the group level analysis (Mikl et al., 2008). We smoothed the data by applying a default 3.00 mm gaussian kernel whose size can be adapted to the monkey brain size using the FSL smooth function (FMRIB's Software Library – FSL, Oxford, U.K) (Smith et al., 2004).

Automatization and Quality Control (QC) report: a basic visual report is generated taking into account alignment accuracy and motion parameters. This report can further be extended using the QAP Python package (https://github.com/preprocessed-connectomes-project/quality-assessment-protocol) that provides measure-of-interest in MRI data quality.

Pypreclin also provides a script to automatically parse and process a *BIDS* (Brain Imaging Data Structure) (Gorgolewski et al., 2016) organized dataset (https://bids.neuroimaging.io), and is built over a smart caching mechanism to speed up the parameters tuning stage. The *Pypreclin* Python package is available on GitHub (https://github.com/neurospin/pypreclin), on the Python Package Index (PyPI) for easy installation and upgrading (https://pypi.org/project/pypreclin), and has been made available as a Singularity container (http://biodev.cea.fr/pypreclin/pypreclin-ubuntu.simg). *Pypreclin* pipeline is fully automatic, but it allows for a manual initialization. In this aim, where total automatization can lead to unsolvable mistakes without modifying the code, we overcome this limit by freely tuning the alignment in graphical or command line mode. The processing time of Pypreclin pipeline is about few hours, depending on the images parameters and the computational ressources. For example, it required approximately 5 hours to preprocess 500 functional brain volumes acquired at 3T with a resolution of 1.25 mm^3 voxel size using 8 CPUs.

2.5. Comparison with the former NeuroSpin Macaque (NSM) fMRI preprocessing

We previously developed a preprocessing pipeline for contrast enhanced monkey fMRI acquired in awake (Uhrig et al., 2014; Wang et al., 2015) or anesthetized macaques (Barttfeld et al., 2015; Uhrig et al. 2016, 2018). This is referred as '*NSM*' for 'NeuroSpin Macaque' pipeline. The differences between NSM and *Pypreclin* pipelines are highlighted in Table 1.

Slice timing and realignment steps are identical in both NSM and *Pypreclin* pipeline.

B_0 inhomogeneities correction: NSM preprocessing rigidly correct B_0 inhomogeneities slice by slice (2 dimensions) (ITK ImageRegistrationMethod function) (Yoo et al., 2002).

Reorientation: NSM can only apply one type of transformation for reorientation assuming that acquisitions are always made in the sphynx position. In comparison, *Pypreclin* can reorient images regardless of the monkey's position during fMRI acquisition.

Normalization and B_1 inhomogeneities correction: NSM preprocessing does not use the monkey's own anatomical image, but rather directly coregisters the chosen template image (e.g. macaque MNI template) (Frey et al., 2011) with the functional images.

Masking: only an erosion function using FSL bet2 (Smith et al., 2004) was applied to remove some extra-brain signal (such as muscle) and facilitate the coregistration.

Coregistration: the NSM preprocessing overlays reference and functional images using the FSL flirt function with affine transformation (Smith et al., 2004).

Smoothing: data are smoothed with a 3.00 mm isotropic gaussian kernel (the third of human size) using the scipy gaussian_filter function (http://www.scipy.org/) (Jones et al., 2001).

Automatization and Quality Control (QC) report: NSM preprocessing is fully automatic with no possibility of manual initialization and does not provide a quality check reporting.

2.6. Corrections and alignment

To assess alignment accuracy, we computed normalized Mutual Information (nMI) between images (Kraskov et al., 2004). The nMI value corresponds to the value of the mutual dependence between two images A and B for which we smoothed the joint histogram with a gaussian filter. The theoretical maximum nMI value corresponds to the case where both images A and B are the macaque template image. We discriminated it from the practical maxima nMI values evaluated between the T1 image and the MNI macaque template image (anatomical on template) (Frey et al., 2011). Finally, the nMI was calculated between the coregistered functional images and the MNI macaque template image (Frey et al., 2011). We then applied a Student t-test on the mean nMI between the NSM preprocessing and the *Pypreclin* preprocessing for all the 9 conditions (Fig. 2).

For alignment and masking, we overlay the MNI macaque template on coregistered functional images for both NSM and *Pypreclin* preprocessing for all experimental conditions. By explicit visual checking, we reported results with 'Success' or 'Failure' (Fig. 3 and S2, S3). Visual processing reports involved the assessment of five quality checkpoints (alignment of template iso-value lines with sulcus contrasts on functional images; amount of voxels outside the template; translation between the template image and the EPI images; rotation between the template image and the EPI images and field of view overflow) and 'Success' was defined for a minimal score of 4 over 5.

Finally, we tested the effect of the template by preprocessing functional images with *Pypreclin* using five macaque brain templates: D99 (Reveley et al., 2017), CIVM (Calabrese et al., 2015a,b), NMT (Seidlitz et al., 2018), INIA19 (Rohlfing et al., 2012) and MNI (Frey et al., 2011). We displayed the coregistered functional images onto the isocontour map template (Fig. 8A).

2.7. Statistical analysis of auditory evoked fMRI

The statistical first level analysis was performed with Nistats Python module (https://nistats.github.io/index.html) using a Generalized Linear Model (GLM) (Abraham et al., 2014) and consisted in 3 conditions (habituation of either low or high frequency sound trials, rare and frequent low or high frequency sound trials) for sounds and their associated derivatives. We also added motion regressors as variables of non

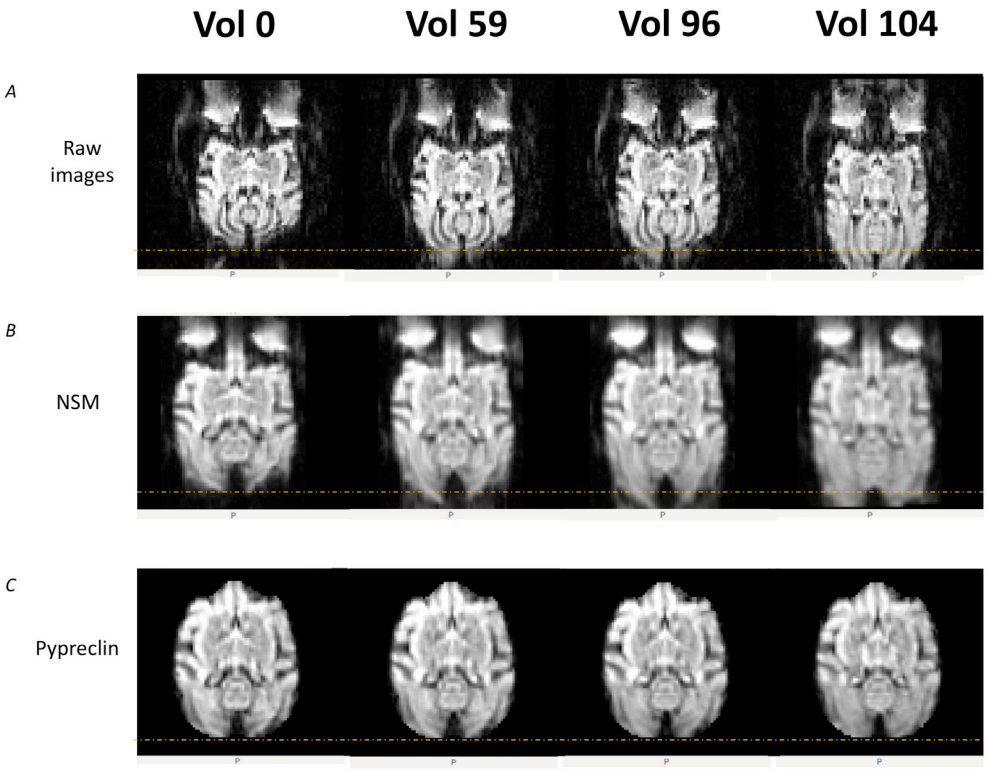

Fig. 1. Example of distortions occurring in the phase-encoding direction and preprocessing corrections during an awake scanning session. Transversal slices show B_0 inhomogeneities (raw images, top panel - A) and their corrections after applying the NeuroSpin Monkey preprocessing (NSM, middle panel - B) or the *Pypreclin* preprocessing (lower panel - C) on MION fMRI data acquired with a single channel coil 1Tx-1Rx (mono coil) in the awake state.

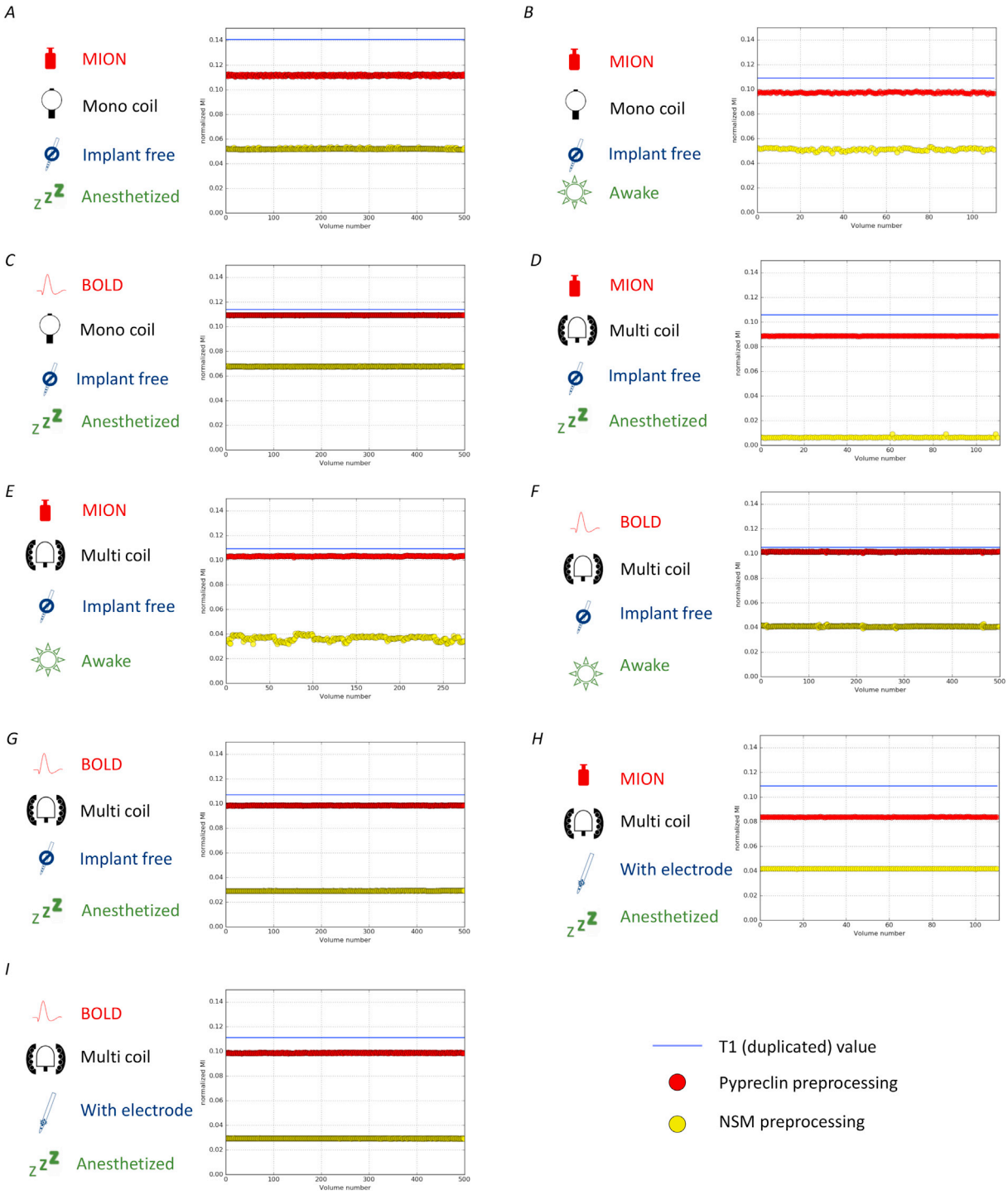

Fig. 2. Comparison of motion correction and normalization between the NeuroSpin Monkey (NSM) and the *Pypreclin* preprocessing, assessed with normalized Mutual Information (nMI). Normalization (blue) and coregistration values for the NeuroSpin Monkey pipeline (NSM, yellow), and the *Pypreclin* pipeline (red) are computed. (A) MION fMRI data acquired with a single channel coil 1Tx-1Rx (mono coil) under anesthesia; (B) MION fMRI data acquired with a single channel coil 1Tx-1Rx (mono coil) in the awake state; (C) BOLD fMRI data acquired with a single channel coil 1Tx-1Rx (mono coil) under anesthesia; (D) MION fMRI data acquired with a multichannel phased-array 1Tx-8Rx coil (multi coil) under anesthesia; (E) MION fMRI data acquired with a multichannel phased-array 1Tx-8Rx coil (multi coil) in the awake state; (F) BOLD fMRI data acquired with a multichannel phased-array 1Tx-8Rx coil (multi coil) in the awake state; (G) BOLD fMRI data acquired with a multichannel phased-array 1Tx-8Rx coil (multi coil) under anesthesia; (H) MION fMRI data acquired with a multichannel phased-array 1Tx-8Rx coil (multi coil) under anesthesia with intracranial implanted device (electrode); (I) BOLD fMRI data acquired with a multichannel phased-array 1Tx-8Rx coil (multi coil) under anesthesia with intracranial implanted device (electrode).

interest in the model to compute a Z map per run (Fig. S10). Activation time was modeled within each fMRI run with the MION hemodynamic response function (HRF) (Vanduffel et al., 2001). Beta weight images of activations for the awake and anesthetized condition expressed signal change for all sounds relative to silence periods. Each single level image was computed at a statistical threshold of $p < 0.001$ uncorrected at the voxel level. We studied cerebral activations on the whole brain considering all fMRI voxels. We then included all the runs in a second level

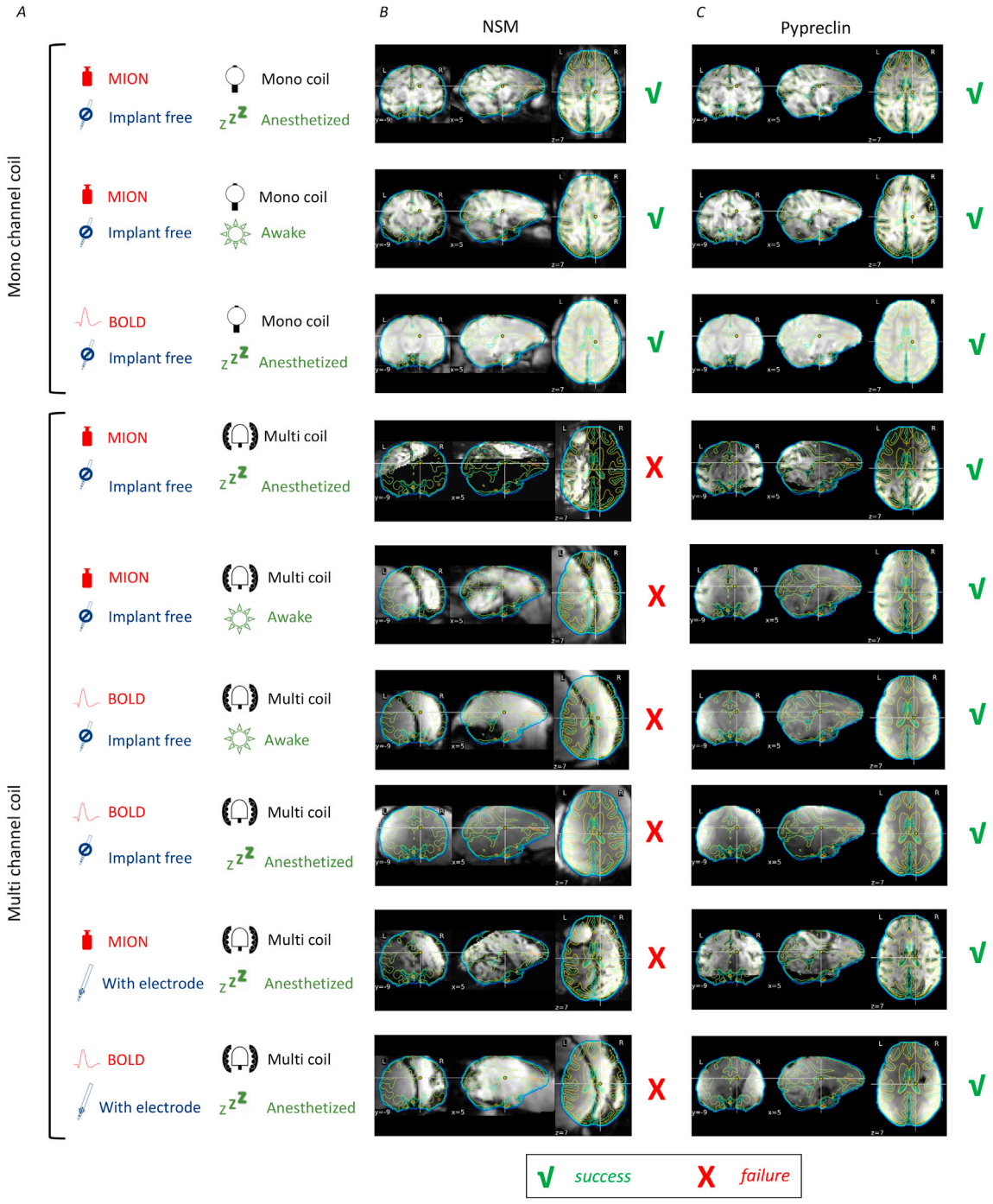

Fig. 3. Preprocessing output visual reports in all acquisition condition (A) for the NeuroSpin Monkey pipeline (NSM; B) and the *Pypreclin* pipeline (C). The MNI template (Frey et al., 2011) is overlaid with an isocolor map on each functional image. Success and failures of the coregistration are reported.

ANOVA and reported values of $p < 0.05$ Bonferroni corrected at the voxel level.

2.8. Brain areas labeling

The CIVM atlas (template and labels) (Calabrese et al., 2015a,b) was warped to the MNI macaque space (Frey et al., 2011). We implemented the CIVM parcellation of 241 ROIs to directly recover brain regions names and accurately localize clusters obtained from volumetric analysis. This step is performed using FSL eyes function (https://zenodo.org/record/2630502: McCarthy Paul; 2019 April 5; FSLeyes Version 0.28.0).

2.9. PRIME-DE dataset

To evaluate *Pypreclin* robustness and rule out a single site effect, we challenged the *Pypreclin* pipeline with fMRI data collected from 14 other imaging sites in different international institutions, using distinct scanners/magnetic fields/coils/fMRI protocols/macaque species. Institutions were as follow: Lyon Neuroscience Research Center (abbreviated as *Lyon* in figures), Princeton, Nathan Kline Institute (abbreviated as *NKI* in figures), Netherlands Institute for Neuroscience (abbreviated as *NIN* in figures), University of California Davis (abbreviated as *UC Davis* in figures), Newcastle, East China Normal University Kwok (abbreviated as *ECNU_K* in figures), University of Western Ontario (abbreviated as *UWO*

in figures), Mount Sinai Philips (abbreviated as *MT Sinai_P* in figures), University of Minnesota (abbreviated as *UMN* in figures), Institute of Neuroscience (abbreviated as *IoN* in figures), Steam cell and Brain Research Institute (abbreviated as *SBRI in* figures) and Rockefeller. These datasets are now made available thanks to the Primate neuroimaging Data-Exchange (PRIME-DE) monkey fMRI data sharing initiative which have been recently introduced to develop open resources for non-human primate imaging (Milham et al., 2018). We included data for which both anatomical and functional images were available and free of Data Usage Agreement. We tested the preprocessing pipeline on BOLD or MION fMRI images acquired on two macaque species (*macaca mulatta* and *fascicularis*) in the awake state or under anesthesia. Monkeys were scanned at different magnetic field strengths (1.5, 3.0, 4.7 and 7.0T) using four distinct scanner manufacturers (Brucker, Germany; Philips, Netherlands; Siemens, Germany and undisclosed) and four categories of coils: i) mono channel coil (abbreviated as *Mono coil* in the figures), ii) multichannel phased-array coil (abbreviated as *Multi coil* in the figures), iii) clinical body coil (abbreviated as *Body coil* in the figures) and iv) clinical knee coil (abbreviated as *Knee coil* in the figures).

Each functional scan consisted of EPI sequence with a repetition time (TR) between 1000 and 3000 ms. The spatial resolution varied from 1 mm isotropic to 2*2*3 mm^3 voxel size. There were between 160 and 988 brain images per run. Anatomical scans consisted of T1 sequence with an Inversion Time (TI) of 750 to 1000 ms and a spatial resolution of 0.47 to 1.00 isotropic mm^3 voxel size. Full details are provided in the Supplementary Tables 6 and 7

We assessed the correction and alignment step as described in section 2.6 by computing the normalization and coregistration normalized Mutual Information (nMI) metric. For the functional time serie (coregistration), we reported the mean and standard deviation of nMI to assess the quality of the preprocessed functional images (Fig. 6). Similarly, we overlaid the coregistered functional images and the MNI macaque template (Frey et al., 2011) for each site included from the PRIME-DE database (Fig. 7).

Finally, we tested the effect of the template by preprocessing functional images with *Pypreclin* using five macaque brain templates as reported in section 2,6 and displayed the results for one dataset (Fig. 8B).

3. Results

3.1. Comparison between the Pypreclin and the former NSM fMRI preprocessing pipeline (Neurospin dataset)

3.1.1. Distortion and motion correction

The theoretical maximum nMI value for the MNI macaque template was 0.443. Practical maxima were given by anatomical images compared to the MNI macaque atlas (Frey et al., 2011), for which nMI varied between 0.10 and 0.14 with a maximum for the first condition (MION - 1Tx-1Rx - Implant free - Anesthetized). This anatomical to template nMI was reported as a blue asymptote for each acquisition condition (Fig. 2). The mean normalized mutual information for the functional images to the MNI macaque template obtained for the NSM preprocessing was 0.0521 (yellow points) whereas with *Pypreclin*, the nMI reached 0.1118 for the same associated condition (red dots) (Fig. 2A). Respectively through all other conditions, nMI values were: nMI NSM = 0.0511 and nMI *Pypreclin* = 0.0973 (MION - 1Tx-1Rx - Implant free – Awake, Fig. 2B); nMI NSM = 0.0677 and nMI *Pypreclin* = 0.1094 (BOLD - 1Tx-1Rx - Implant free – Anesthetized, Fig. 2C); nMI NSM = 0.0064 and nMI *Pypreclin* = 0.0887 (MION – 1Tx-8Rx coil - Implant free – Anesthetized, Fig. 2D); nMI NSM = 0.0364 and nMI *Pypreclin* = 0.1032 (MION – 1Tx-8Rx coil - Implant free – Awake, Fig. 2E); nMI NSM = 0.0408 and nMI *Pypreclin* = 0.1013 (BOLD – 1Tx-8Rx coil - Implant free – Awake, Fig. 2F); nMI NSM = 0.0292 and nMI *Pypreclin* = 0.0985 (BOLD – 1Tx-8Rx coil - Implant free – Anesthetized, Fig. 2G); nMI NSM = 0.0418 and nMI *Pypreclin* = 0.0838 (MION – 1Tx-8Rx coil – With electrode – Anesthetized, Fig. 2H) and nMI NSM = 0.0293 and nMI *Pypreclin* = 0.0987 (BOLD – 1Tx-8Rx coil – With electrode – Anesthetized, Fig. 2I). Applying a statistical Student *t*-test on the NSM and *Pypreclin* mean nMI, the result was always significant ($p < 1e\text{-}6$). *Pypreclin* performed around 3.7 times better than the NSM preprocessing based on the mean nMI scores ($h = 1$ with $p < 1.3e\text{-}6$ for Student *t*-test on mean NSM and *Pypreclin* across all conditions).

3.1.2. Quantifying success and alignment with the MNI macaque template

The NSM preprocessing could only achieve successful preprocessing for 3 experimental conditions (corresponding to acquisitions performed with the mono channel coil) whereas *Pypreclin* could successfully achieve the preprocessing in all the 9 experimental conditions (Fig. 3). Where both preprocessing manages to correctly coregister functional images with the MNI macaque template (Frey et al., 2011), the *Pypreclin* pipeline displays a closer overlay for different sulci and gyri compare to NSM pipeline (Fig. 4 and Supplem S2 and S3), especially for the awake acquisitions.

3.1.3. Task-evoked fMRI in awake macaques

We tested auditory stimuli versus silence periods in awake fixating macaques. Using the NSM preprocessing pipeline, we found fMRI activations in the auditory cortex, belt and parabelt regions including medial and lateral part of the auditory koniocortex (A1 or AKM, $Z_{left} = 5.04$ and $Z_{right} = 5.18$; AKL, $Z_{left} = 5.17$), in caudal part of the paraauditory area (PaAC, $Z_{left} = 5.13$ and $Z_{right} = 5.08$), in prokoniocortex (ProK, $Z_{right} = 5.08$) in granular insular cortex (GI, $Z_{right} = 5.16$), in the temporal parietooccipital associated area in STS (TPO, $Z_{left} = 5.33$) and bilaterally in the cerebral white matter (CWM, $Z_{left} = 5.33$ & $Z_{right} = 5.16$). 121 voxels were localized within the left cerebral white matter and 77 within the right cerebral white matter.

Using *Pypreclin* pipeline, we found fMRI activations within the auditory cortex, belt and parabelt regions, including medial and lateral part of the auditory koniocortex (A1 or AKM, $Z_{left} = 4.99$ and $Z_{right} = 5.40$; AKL, $Z_{left} = 4.91$ and $Z_{right} = 5.06$), in caudal and lateral part of the paraauditory area (PaAC, $Z_{left} = 5.03$ and PaAL, $Z_{right} = 5.03$), in medial and lateral part of the prokoniocortex (ProKM, $Z_{right} = 5.26$ and ProKL, $Z_{right} = 5.37$), in the granular and dysgranular insular cortex (GI, $Z_{right} = 5.31$ & DI, $Z_{right} = 5.39$), in temporal area (Taa, $Z_{right} = 4{,}90$), in opercular part of the parietal area (PGOp, $Z_{left} = 5.08$), in the secondary somatosensory cortex including internal and external part (S2, $Z_{left} = 5\ 00$ and $Z_{right} = 5.02$; S2I S2I, $Z_{right} = 5.26$; S2E, $Z_{right} = 5.24$), in superior temporal sulcus 3 (ST3, $_{right} = 4.97$) and bilaterally in the cerebral white matter (CWM, $Z_{left} = 5.02$ & $Z_{righ} = 5.17$). 40 voxels were localized within the left cerebral white matter and 36 within the right cerebral white matter (Fig. 5A, and Supplem S4 to S6; Table S4).

3.1.4. Task-evoked fMRI in anesthetized macaques

We tested the same auditory stimuli versus silence periods in anesthetized macaques. Using the NSM preprocessing pipeline, we found bilateral fMRI activations localized in the auditory cortex, belt and parabelt regions, including medial and lateral part of the auditory koniocortex (A1 or AKM, $Z_{left} = 6.81$ and $Z_{right} = 6.11$; AKL, $Z_{left} = 5.29$ and $Z_{right} = 5.84$), in the caudal part of the paraauditory area (PaAC, $Z_{left} = 5.88$ & $Z_{right} = 5.91$), in the prokoniocortex (ProK, $Z_{left} = 6.19$ & $Z_{right} = 5.68$), in the granular insular cortex (GI, $Z_{left} = 5.94$ & $Z_{right} = 5.71$), in the temporal parietooccipital associated area in STS (TPO, $Z_{left} = 5.77$ & $Z_{right} = 5.21$), in the temporal part of the retroinsular area (ReIT, $Z_{left} = 5.20$ & $Z_{right} = 5.54$), in the secondary somatosensory cortex (S2, $Z_{left} = 5.51$ & $Z_{right} = 5.48$), and in the cerebral white matter (CWM, $Z_{left} = 6.29$ & $Z_{right} = 5.72$). Activations were also observed in the left hemisphere uniquely, including lateral part of the paraauditory cortex (PaAL, $Z_{left} = 5.62$), medial and lateral part of the prokoniocortex (ProKM, $Z_{left} = 5.44$ and ProKL, $Z_{left} = 5.59$), the temporal area (TaA, $Z_{left} = 5.48$), the occipitomedial part of the temporal area (TEOM, $Z_{left} = 4.98$), the superior temporal sulcus 3 (ST3, $Z_{left} = 5.50$), the temporoparietal cortex (Tpt, $Z_{left} = 5.57$), the external and internal part of the secondary

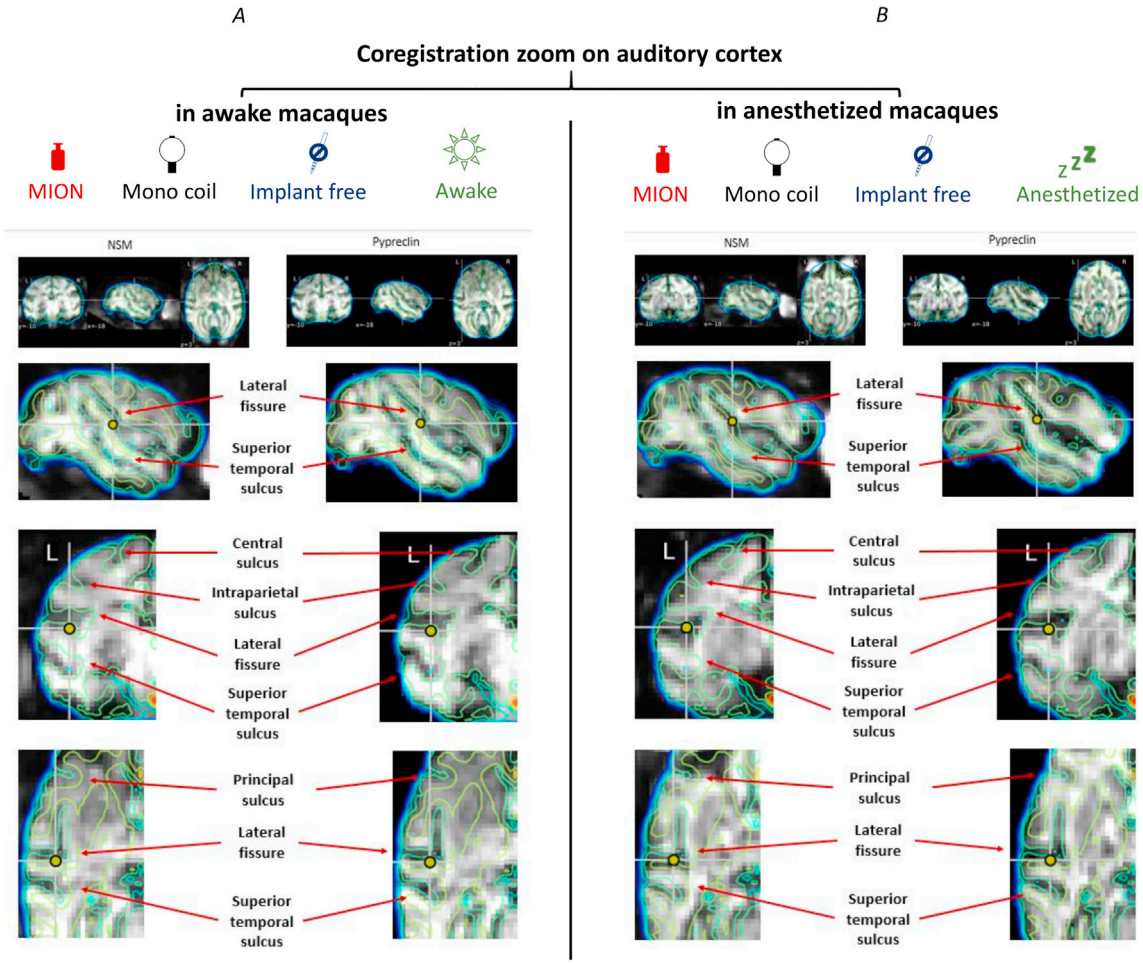

Fig. 4. Coregistration of the auditory cortex from functional images preprocessed with the NeuroSpin Monkey preprocessing (NSM) or the *Pypreclin* preprocessing overlaid to the MNI macaque template. The MNI macaque template (Frey et al., 2011) is overlaid with an isocolor map for sagittal, coronal and axial slices with focus on the lateral fissure, superior temporal sulcus, central sulcus and principal sulcus on MION fMRI data acquired either under anesthesia (left – A) or in an awake monkey (right – B) with a single channel coil 1Tx-1Rx (mono coil).

somatosensory cortex (S2I, $Z_{left} = 5.78$ and S2E, $Z_{left} = 5.51$) and the middle temporal visual area 5 (MT_V5, $Z_{left} = 5.23$). 320 voxels were localized within the left cerebral white matter and 156 within the right cerebral white matter.

Using *Pypreclin*, we found bilateral fMRI activations in the auditory pathway within auditory cortex, belt and parabelt regions, including medial and lateral part of the auditory koniocortex (A1 or AKM, $Z_{left} = 5.48$ and $Z_{right} = 6.11$; AKL, $Z_{left} = 5.29$ & $Z_{right} = 5.84$), caudal part of the paraauditory cortex (PaAC, $Z_{left} = 5.28$ & $Z_{right} = 5.73$), the prokoniocortex and the medial part (ProK, $Z_{left} = 5.30$ and $Z_{right} = 5.56$; ProKM, $Z_{left} = 4.95$ and $Z_{right} = 5.16$), the granular insular cortex (GI, $Z_{left} = 5.40$ and $Z_{right} = 5.25$), the temporal parietooccipital area in sts (TPO, $Z_{left} = 5.01$ and $Z_{right} = 5.46$), the temporoparietal cortex (Tpt, $Z_{left} = 5.04$ and $Z_{right} = 5.36$), the secondary somatosensory cortex and the internal and external part (S2, $Z_{left} = 5.17$ and $Z_{right} = 5.47$; S2I, $Z_{left} = 5.43$ and $Z_{right} = 5.46$; S2E, $Z_{left} = 5.23$ & $Z_{right} = 5.38$), the putamen (Pu, $Z_{left} = 5.13$ & $Z_{right} = 4.98$), the hypothalamus (Hy, $Z_{left} = 5.43$ & $Z_{right} = 5.24$) and the cerebral white matter (CWM, $Z_{left} = 5.27$ & $Z_{right} = 5.62$). Activations were also observed in the right hemisphere uniquely, including lateral part of the paraauditory cortex (PaAL, $Z_{right} = 5.17$), occipitomedial part of the temporal area (TEOM, $Z_{right} = 5.08$), retroinsular area and the temporal part (ReI, $Z_{right} = 4.96$; ReIT, $Z_{right} = 5.04$), opercular part of the parietal area (PGOp, $Z_{right} = 5\ 0.03$), the insular proisocortex (Ipro, $Z_{right} = 5.29$) and the middle temporal visual area 5 (MT_V5, $Z_{left} = 5.37$), or in the right hemisphere only for lateral part of the prokoniocortex (ProKL, $Z_{left} = 5.00$). 197 voxels were localized within the left cerebral white matter and 293 within the right cerebral white matter (Fig. 5B and Supplem S7 to S9; Table S5).

3.2. *Pypreclin results on the Prime-DE dataset*

3.2.1. *Distortion and motion correction*

The theoretical maximum nMI value was 0.443. Practical maxima nMI were computed between the anatomical image and the MNI macaque atlas (Frey et al., 2011) and varied from 0.1174 to 0.1743. This value was reported as a blue triangle for each center (Fig. 6). Respectively through all centers, mean nMI normalization values were: nMI Lyon = 0.1214; nMI Princeton = 0.1555; nMI NKI = 0.1304; nMI NIN = 0.1331; nMI UC Davis = 0.1241; nMI Newcastle = 0.1294; nMI ECNU_K = 0.1360; nMI UWO = 0.1174; nMI MT Sinai_P = 0.1411; nMI OHSU = 0.1743; nMI UMN = 0.1371; nMI IoN = 0.1567; nMI SBRI = 0.1638 and nMI Rockefeller = 0.1224. The mean nMI between the functional images and the MNI macaque template varied between 0.1093 and 0.1221 and were reported as red dots for each center (Fig. 6). For all the centers, mean nMI coregistration values were: nMI Lyon = 0.1210 (1.5T, MION, Awake, Body coil); nMI Princeton = 0.1219 (3T, BOLD, Anesthetized, Body coil); nMI NKI = 0.1191 (3T, MION, Awake, Multi coil); nMI NIN = 0.1195 (3T, BOLD, Anesthetized, Multi coil); nMI UC Davis = 0.1093 (3T, BOLD, Anesthetized, Multi coil); nMI Newcastle = 01149 (4.7T, BOLD, Awake, Multi coil).; nMI ECNU_K = 0.1221 (3T, BOLD, Anesthetized, Mono coil); nMI UWO = 0.1120 (7T, BOLD, Anesthetized, Multi coil); nMI MT Sinai_P = 0.1209 (3T, BOLD, Anesthetized, Body coil); nMI

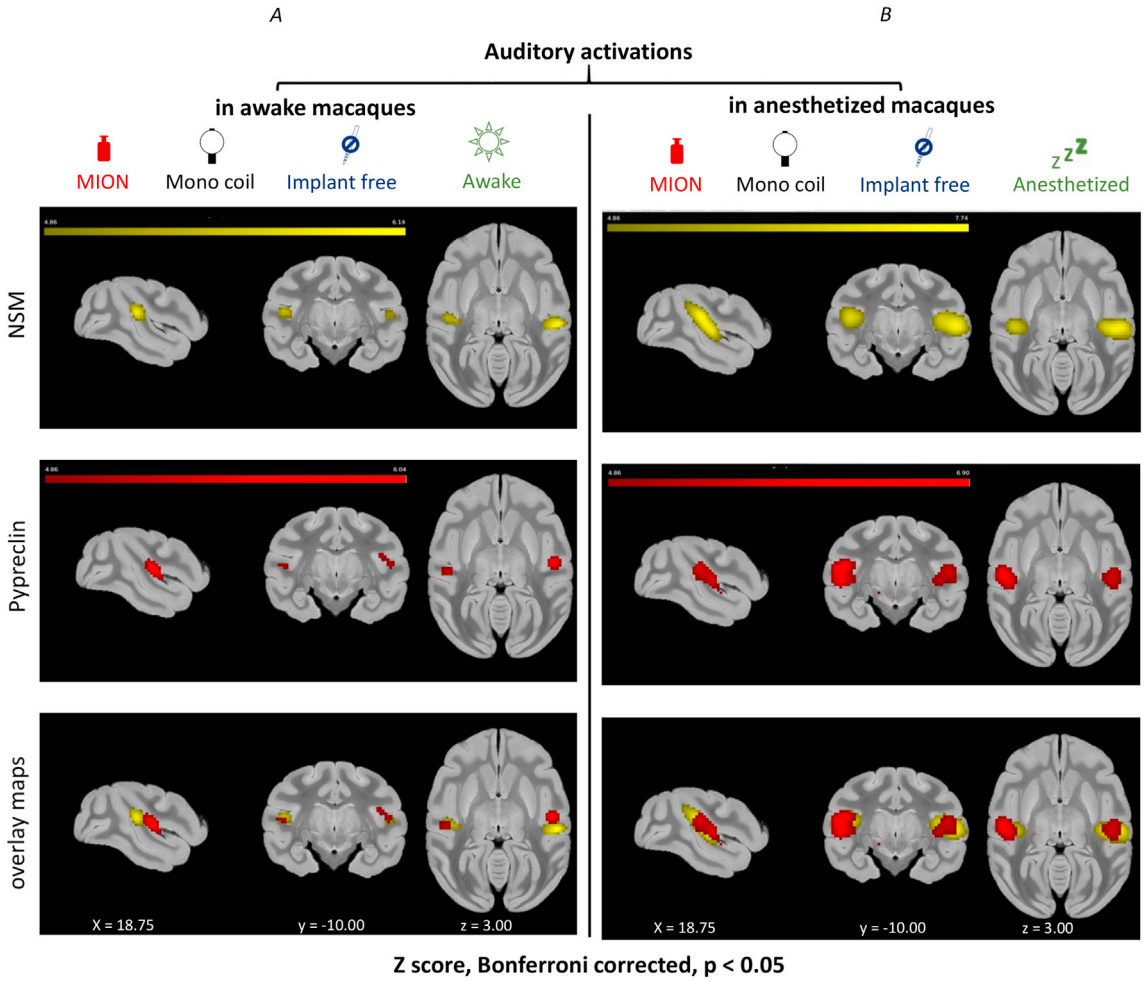

Fig. 5. fMRI activation maps for the auditory task using the NeuroSpin Monkey (NSM, yellow) or the *Pypreclin* preprocessing (red). Data were acquired using contrast agent-enhanced fMRI (MION) with a single-loop 1Tx-1Rx coil (mono coil) in the awake state (left, A) or under anesthesia (right, B). Statistical maps are displayed as sagittal, coronal and axial views, on the level of primary auditory cortex. Maps are obtained following the NSM preprocessing (upper panels) or the *Pypreclin* preprocessing (middle panels), and overlaid (lower panels).

OHSU = 0.1121 (3T, BOLD, Anesthetized, Knee coil); nMI UMN = 0.1106 (7T, BOLD, Anesthetized, Multi coil); nMI IoN = 0.1185 (3T, BOLD, Anesthetized, Multi coil); nMI SBRI = 0.1213 (3T, BOLD, Anesthetized, Body coil) and nMI Rockefeller = 0.1184 (3T, MION, Anesthetized, Multi coil).

Thus, *Pypreclin* successfully preprocessed fMRI images in all the 19 experimental conditions for the PRIME-DE dataset (Fig. 7).

3.3. Role of the macaque template

Pypreclin is a flexible tool that allows users to provide any template as an input parameter. *Pypreclin* successfully preprocessed fMRI data from both the NeuroSpin Center dataset and the PRIME DE database with each of the five tested macaque templates: D99 (Reveley et al., 2017), CIVM (Calabrese et al., 2015a,b), NMT (Seidlitz et al., 2018), INIA19 (Rohlfing et al., 2012) and MNI (Frey et al., 2011) (Fig. 8).

4. Discussion

Pypreclin is a new versatile preprocessing pipeline that addresses the challenges raised by macaque fMRI. *Pypreclin* robustly succeeded data preprocessing in several distinct experimental settings such as awake fMRI (with movement induced artifacts), anesthesia fMRI, BOLD fMRI, iron oxide contrast agent fMRI, using either a single loop or a phased-array coil, and in animals previously implanted with metallic intracranial electrodes. Moreover, *Pypreclin* could also preprocess fMRI data from distinct international sites using different protocols and hardwares. Thus, *Pypreclin* is a good candidate for generating standardized data analysis pipelines in the non-human primate fMRI community (Milham et al., 2018).

4.1. Specific challenges in the preprocessing of macaque fMRI data

Macaque fMRI raises several challenges that increase the difficulty of monkey images preprocessing. The first challenge is related to body motion during awake imaging. Although macaques have their head fixed during acquisition and are generally trained in a mock scanner to improve their behavior and minimize motions prior to actual scanning (Vanduffel et al., 2001; Uhrig et al., 2014), they are still prone to body motions and to chewing movements when they receive fluids as a reward, which induce distortions and ghosting within images (Keliris et al., 2007). It has been demonstrated that monkeys body and jaw movements do not displace the fixed head but rather induce changes in B_0 which strongly affect signal stability and statistical maps (Keliris et al., 2007). Compared to human fMRI, this is a particularity to monkey fMRI that needs to be addressed specifically during data preprocessing. In fact, body movements lead to B_0 inhomogeneities with a specific source of artifacts, which will increase with the B_0 strength (Keliris et al., 2007; Orban et al., 2003). To address this specific challenge, it is key to extensively train monkeys in a mock scanner before real fMRI

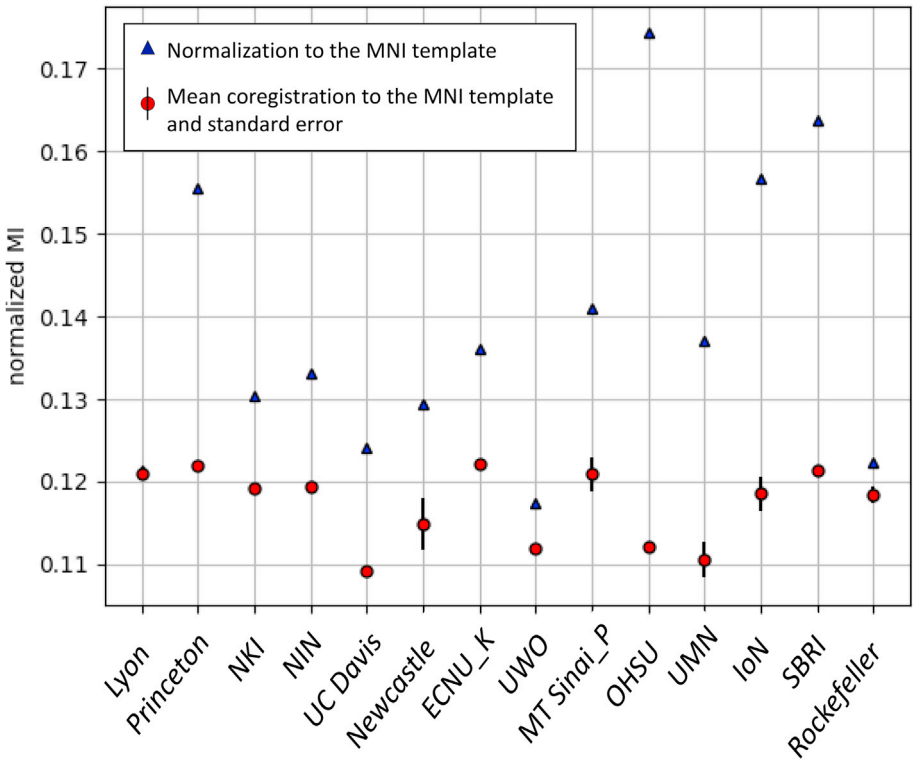

Fig. 6. Assessment of motion correction and normalization of PRIME-DE dataset using normalized Mutual Information (nMI) after the *Pypreclin* preprocessing. Normalization (blue triangle) and coregistration values with standard error (red dots) are computed for images where centers provided both anatomical and functional scans free of Data Usage Agreement.

acquisition, preferably in the sphinx position (Valette et al., 2006). However, this is still not enough to reduce the distortions induced by body and jaw movements. *Pypreclin* addressed this challenge by using advanced normalization tools (ANTS) (Keliris et al., 2007; Avants et al., 2011).

Removing extra-brain signals (muscles and skull bones) is mandatory to guide the registration step. However, the contrast between the brain and the non-brain tissue is not trivial in monkey images. Despite the community efforts to develop adapted methods for macaque fMRI (Table 2), it remains challenging and no single method is able to handle all variability of the monkey's images. The challenge is even greater when data are acquired in awake behaving macaques or with metallic sources of artifacts such as those generated by intracranial electrodes. Whereas the NSM preprocessing uses FSL bet2 function, no generic settings were found to correctly remove all of the non-brain tissue without cutting any cortical area on the large panel of tested images. Milham et al., (2018) proposed a switch from AFNI 3dSkullstrip to the combination of FSL bet2 and AFNI 3dAutomask, according to each dataset. Here we aimed at introducing a single universal approach that does not consider non-brain tissues removal as a segmentation issue. In *Pypreclin*, we wrap the mask defined on the template using the deformation obtained during the registration procedure. We demonstrated that this method is highly reproducible (Figs. 3 and 7).

4.2. Comparison with a previous preprocessing pipeline

Whereas our previous NSM pipeline successfully achieved data preprocessing in the previously applied experiments (MION fMRI, monochannel 1TxRx coil, with no implanted metallic electrodes) (Uhrig et al., 2014; Wang et al., 2015; Barttfeld et al., 2015; Uhrig et al., 2016), only the new *Pypreclin* preprocessing could achieve robust preprocessing in the extended panel of experimental conditions. There are several structural differences in the way the two pipelines analyze MRI images that could account for this discrepancy in results and the versatility of *Pypreclin*. *Pypreclin* corrects for B_0 field inhomogeneities using nonlinear correction, performs a normalization between the template and T1 image before correcting B_1 field inhomogeneities, while NSM corrects for B_0 field inhomogeneities using rigid linear correction, directly coregisters the chosen template image with the functional images, not taking in account the anatomical T1 image.

Non-linear transformation: Monkey movements generate inhomogeneities in the magnetic field and especially during the awake sessions (Keliris et al., 2007; Pfeuffer et al., 2007; Orban et al., 2003). The expected higher distortions are better corrected using non-linear transformation in the phase-encoding direction (*Pypreclin* preprocessing) compared to a 2D rigid transformation (NSM preprocessing). These results suggest that signal distortions within the macaque brain are not homogeneous and thus corroborate the interest of using a diffeomorphism transformation as shown by Avants and colleagues (Avants et al., 2011) (Fig. 1 and Supplem S12).

Normalization & B_1 field corrections: Pypreclin preprocessing performs a normalization between the template and T1 image before correcting B_1 field inhomogeneities. This order facilitates masking and alignment steps but corrects low frequency intensity nonuniformity once the normalization done. *Pypreclin* pipeline is built in a flexible manner and provides the opportunity to repeat this step. This implementation can act through a loop to recover outputs from B_1 field corrections and apply once again the normalization between the anatomical image and the template.

Masking step: two different strategies to mask extra brain signal were implemented. NSM preprocessing do not generated a mask and applied it only during the statistical analysis. *Pypreclin* preprocessing generates a mask on both native and template images before any statistical analysis. The use of a non-linear normalization between the anatomical and template image (as implemented in *Pypreclin* pipeline) requires the creation of a mask, which is extended to anatomical and functional images in all coordinate systems. Computing the mask for each MRI sequence minimizes errors, avoids averaging during statistical analysis and allows to work in the native space (Caballero-Gaudes and Reynolds, 2017)

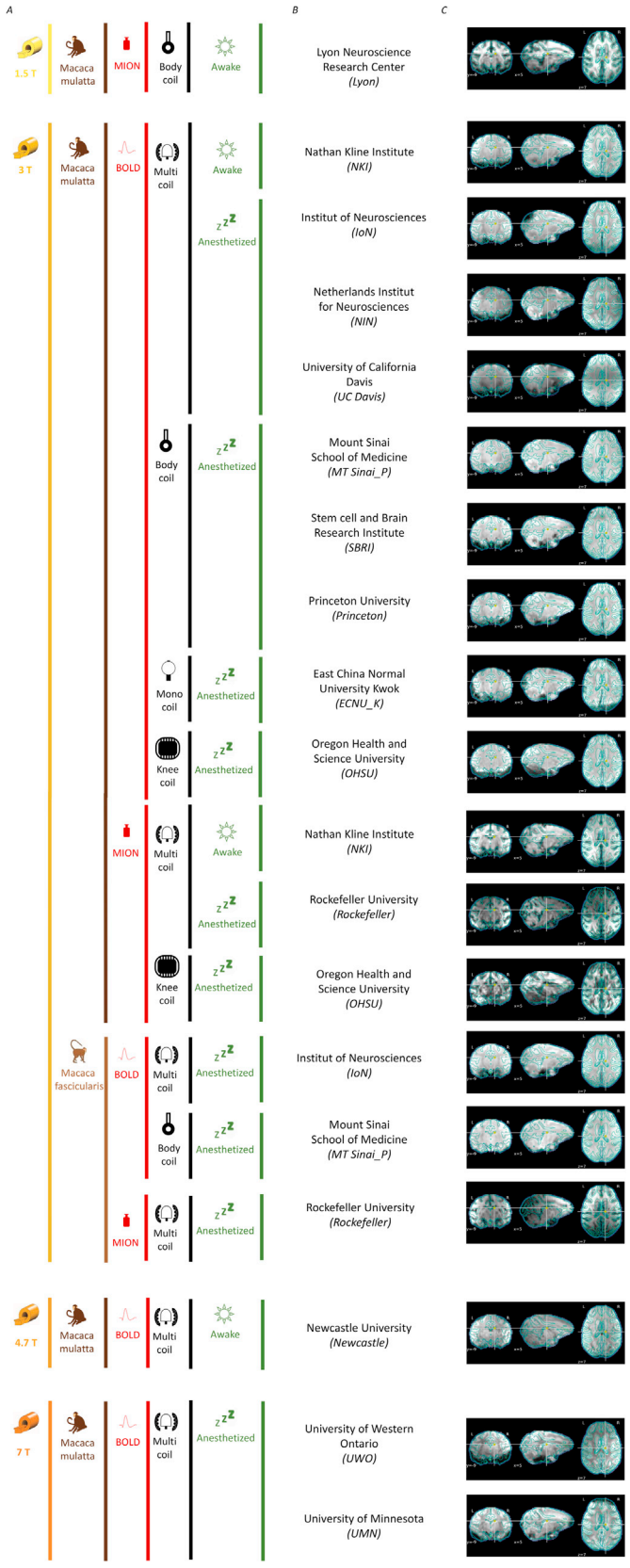

Fig. 7. Results of the *Pypreclin* preprocessing (C) for different experimental conditions (A) of PRIME-DE database (B). The MNI macaque template (Frey et al., 2011) is overlaid with an isocolor map on each functional image.

(Fig. S14).

Coregistration with the template: for experimental conditions where both NSM and *Pypreclin* preprocessing achieve the coregistration of functional images with the template, sulcus and gyri are better aligned with the atlas for data preprocessed with *Pypreclin* pipeline. This observation is even more critical for the awake dataset where we expect a more difficult preprocessing due to movements of the body. Zooming on the auditory cortex, the gap observed between the functional image and the template is still more important for images preprocessed with the NSM preprocessing compare to the *Pypreclin* pipeline and can cause discrepancies in the localization of fMRI activity (Fig. 2 and S8 to S11).

Cerebral activations: the reported brain activities were consistent with previously published works. Auditory core, belt and parabelt regions were bilaterally observed in this study and join results from Joly and colleagues (Petkov et al., 2006; Joly et al., 2012a; Joly et al., 2012b). Cortical regions distant from auditory cortex, like temporoparietal sulcus (Tpt) are coherent with Kass and Hackett results (Kaas and Hackett, 2000). The activity located in the superior temporal sulcus (ST3), is consistent with previous works from Brewer and colleagues (Brewer and Barton, 2016) and Ortiz-Rio and colleagues (Ortiz-Rios et al., 2015). Finally, somatosensory areas activated during an auditory task are previously reported (Joly et al., 2012b) as well as activations in the occipital cortex.

4.3. Versatility and accuracy of the Pypreclin preprocessing pipeline

Pypreclin is a Python based preprocessing pipeline. Python is a portable, dynamic, extensible, open source language that allows a modular and object-oriented approach to programming. Thus, *Pypreclin* could be accessed and broadly made available in an easy manner.

Although this pipeline does not use new software or creating algorithms, its strength lies in piling up and ordering the most pertinent functions adapted to the macaque within each step, due to standard tools rather than homemade functions (Tables 1 and 2). Furthermore, the fully automatization of *Pypreclin* aims to decrease time spend on preprocessing, but still allows manual intervention by the user.

Another particularity of *Pypreclin* is to preprocess both BOLD and MION fMRI. Since its introduction in the monkey fMRI field, several groups use iron oxide contrast agent (monocrystalline iron oxide nanoparticle, MION) to enhance sensitivity and statistical power of fMRI (Vanduffel et al., 2001). Thus, the monkey fMRI data generally relies either on BOLD or MION technique. *Pypreclin* achieved successful fMRI preprocessing of both BOLD and MION images.

Pypreclin successfully preprocess fMRI data in several challenging experimental conditions such as in animals implanted with metallic electrical stimulation leads or in images acquired with different head coil technologies. Moreover, auditory-evoked fMRI activations in awake macaques were localized with a higher spatial accuracy after *Pypreclin* preprocessing as compared to a previous macaque fMRI preprocessing pipeline (NSM preprocessing). This accuracy mainly implicates the white matter/gray matter separation (Fig. 5). Although NSM preprocessing achieved accurate gray matter localization of activations in the previous studies (Uhrig et al., 2014; Wang et al., 2015), it proved less accurate in the current study especially in the awake fMRI condition. These differences can be explained by the body motion of the animal during the awake scanning, which lead to important B0 inhomogeneities (Fig. 1). One explanation could be that the previous studies were performed with a higher fixation rate threshold (85%), while the new pipeline could achieve accurate localization at lower behavioral mean threshold (80%), leading to even more B_0 inhomogeneities. In fact, lower fixation rate threshold is associated with more body movements and subsequent image distortion (Figs. 1 and 5, Supplem Tables 4 and 5 and Figs. 4–9).

Since we first developed *Pypreclin* using our research site monkey fMRI data (Neurospin dataset), we aimed to generalize its competence across international research sites to rule out site effect. The recent development of data sharing in the monkey fMRI field is key in allowing

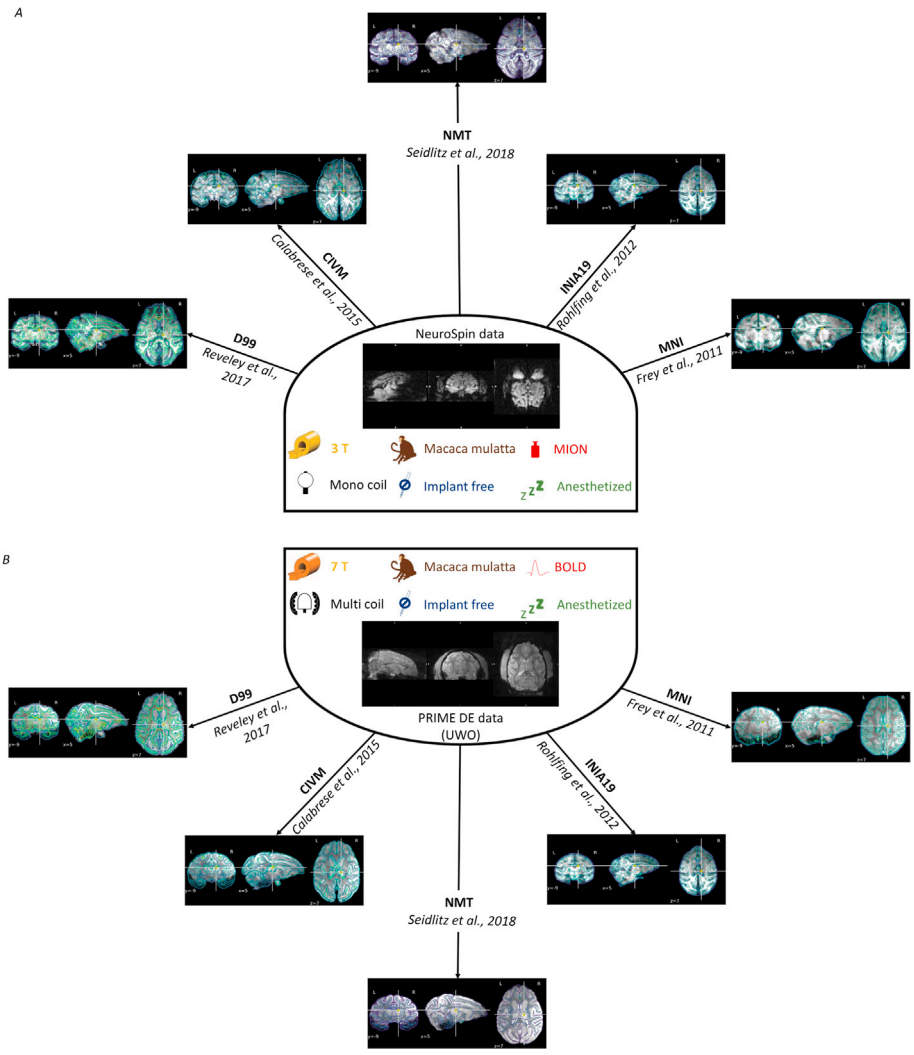

Fig. 8. *Pypreclin* preprocessing outputs using different macaque brain templates. The visual reports overlay the functional image with the D99 template (Reveley et al., 2017), the CIVM template (Calabrese et al., 2015a,b), the NMT template (Seidlitz et al., 2018), the INIA19 template (Rohlfing et al., 2012) and the MNI template (Frey et al., 2011). Two examples are highlighted: (A) NeuroSpin dataset (fMRi data acquired at 3T on *macaca mulatta* under anesthesia with a mono channel coil using MION contrast agent), (B) a PRIME-DE (Milham et al., 2018) dataset from the University of Western Ontario (BOLD fMRI data acquired at 7T on *macaca mulatta* under anesthesia using a multi channel phased-array coil).

quick and easy access to a variety of monkey fMRI data (Milham et al., 2018). A good exemple is the validation that we could achieve by successfully challenging *Pypreclin* on fMRI datasets acquired using different magnetic fields (including ultra-high fields), different hardwares and different protocols. This validation step provides an important piece of evidence for *Pypreclin* versatility and universality, ruling out any site effect.

Futhermore, processing the PRIME-DE dataset emphasize that many sites did not acquire or provide reversed phase-encoded EPI nor field map image, which would prevent the use of TOPUP or FUGUE. *Pypreclin* thus includes these methods as mutually exclusive options.

4.4. Translational applications

One of the great applications of monkey fMRI is the possibility of combining fMRI with intracranial implanted devices such as electrical leads for brain stimulation. Performing fMRI in implanted human subjects became possible only recently and deep brain stimulation devices are approved for MRI with very strict conditions such as 1.5T field (Saenger et al., 2017), with the 3T MRI being performed only in select clinical trials (Boutet et al., 2019). Moreover, artifacts generated by the implanted hardware could lead to take out part of the data such as one hemisphere (Saenger et al., 2017). While our previous classical preprocessing NSM failed to register BOLD images acquired with a monkey implanted with a DBS lead, *Pypreclin* successfully overcame this challenging task.

5. Conclusion

Pypreclin is a new flexible, versatile and robust Python based pipeline for macaque fMRI preprocessing. The entire code is freely available at GitHub (https://github.com/neurospin/pypreclin). Taking in account the recent move toward data sharing in the non-human primate field (Milham et al., 2018), *Pypreclin* can contribute to the standardization effort of fMRI preprocessing among the growing macaque neuroimaging community.

Funding statement

This work was supported by the Fondation pour la Recherche Médicale (FRM grant number ECO20160736100 to JT), Fondation de France, Human Brain Project (Corticity project), Institut National de la Santé et de la Recherche Médicale, Commissariat à l'Energie Atomique, Collège de France, Fondation Bettencourt Schueller.

Author contribution statement

Tasserie: Conceptualization, Methodology, Software, Validation, Formal analysis, Investigation, Resources, Data Curation, Writing - Original Draft, Writing - Review & Editing, Visualization. Grigis: Conceptualization, Methodology, Software, Validation, Formal analysis, Resources, Data Curation, Writing - Original Draft, Writing - Review & Editing, Visualization. Uhrig: Investigation, Writing - Original Draft.

Dupont: Investigation. Amadon: Methodology. Jarraya: Conceptualization, Resources, Writing - Original Draft, Writing - Review & Editing, Visualization, Supervision, Project administration, Funding acquisition.

Declaration of competing interest

The authors declare no competing interests.

Acknowledgments

We thank, Thomas Janssens, Marie-France Hang Foucarde, Michel Luong, Edouard Chazel, Eric Giacomini, Jérémy Bernard, Laurent Laribière, Franck Mauconduit and the NeuroSpin MRI and informatics teams for help with monkey's coils and MRI sequences, Jérôme Cayla, Wilfried Piannezzola and Sébastien Mériaux for help within the animal facility, Timo van Kerkoerle, Qi Zhu, Vincent Frouin and Jean-Robert Deverre for support. We thank Joe Mandeville for his help with the JIP toolbox. We express a special thank to the Primate neuroimaging Data-Exchange (PRIME-DE) initiative, to the organizers and managers of PRIME-DE and to all the institutions that contributed to the PRIME-DE dataset (http://fcon_1000.projects.nitrc.org/indi/indiPRIME.html).

Appendix A. Supplementary data

Supplementary data to this article can be found online at https://doi.org/10.1016/j.neuroimage.2019.116353.

References

Abraham, A., Pedregosa, F., Eickenberg, M., Gervais, P., Mueller, A., Kossaifi, J., Gramfort, A., Thirion, B., Varoquaux, G., 2014. Machine learning for neuroimaging with scikit-learn. Front. Neuroinf. 8, 14.

Absalom, A., Kenny, G., 2005. Paedfusor' pharmacokinetic data set. Br. J. Anaesth. 95, 110.

Autio, Joonas A., Glasser, Matthew F., Ose, Takayuki, Donahue, Chad J., Bastiani, Matteo, Ohno, Masahiro, Kawabata, Yoshihiko, Urushibata, Yuta, Murata, Katsutoshi, Nishigori, Kantaro, Yamaguchi, Masataka, Hori, Yuki, Yoshida, Atsushi, Go, Yasuhiro, Coalson, Timothy S., Jbabdi, Saad, Sotiropoulos, Stamatios N., Smith, Stephen, Van Essen, David C., Hayashi, Takuya, 2019. Towards HCP-style macaque connectomes: 24-channel 3T multi-array coil, MRI sequences and preprocessing. bioRxiv. https://doi.org/10.1101/602979.

Avants, B.B., Tustison, N.J., Song, G., Cook, P.A., Klein, A., Gee, J.C., 2011. A reproducible evaluation of ANTs similarity metric performance in brain image registration. Neuroimage 54, 2033–2044.

Barttfeld, P., Uhrig, L., Sitt, J.D., Sigman, M., Jarraya, B., Dehaene, S., 2015. Signature of consciousness in the dynamics of resting-state brain activity. Proc. Natl. Acad. Sci. U. S. A. 112, 887–892.

Boutet, A., Hancu, I., Saha, U., Crawley, A., Xu, D.S., Ranjan, M., Hlasny, E., Chen, R., Foltz, W., Sammartino, F., Coblentz, A., Kucharczyk, W., Lozano, A.M., 2019. 3-Tesla MRI of deep brain stimulation patients: safety assessment of coils and pulse sequences. J. Neurosurg. 1–9.

Brewer, A.A., Barton, B., 2016. Maps of the auditory cortex. Annu. Rev. Neurosci. 39, 385–407.

Caballero-Gaudes, C., Reynolds, R.C., 2017. Methods for cleaning the BOLD fMRI signal. Neuroimage 154, 128–149.

Calabrese, E., Badea, A., Coe, C.L., Lubach, G.R., Shi, Y., Styner, M.A., Johnson, G.A., 2015a. A diffusion tensor MRI atlas of the postmortem rhesus macaque brain. Neuroimage 117, 408–416.

Calabrese, E., Hickey, P., Hulette, C., Zhang, J., Parente, B., Lad, S.P., Johnson, G.A., 2015b. Postmortem diffusion MRI of the human brainstem and thalamus for deep brain stimulator electrode localization. Hum. Brain Mapp. 36, 3167–3178.

Chen, G., Wang, F., Dillenburger, B.C., Friedman, R.M., Chen, L.M., Gore, J.C., Avison, M.J., Roe, A.W., 2012. Functional magnetic resonance imaging of awake monkeys: some approaches for improving imaging quality. Magn. Reson. Imaging 30, 36–47.

Ekstrom, L.B., Roelfsema, P.R., Arsenault, J.T., Bonmassar, G., Vanduffel, W., 2008. Bottom-up dependent gating of frontal signals in early visual cortex. Science 321, 414–417.

Evans, Dafydd, 2008. A computationally efficient estimator for mutual information. Proc. R. Soc. A Math. Phys. Eng. Sci. 464, 1203–1215.

Fischmeister, F.P., Hollinger, I., Klinger, N., Geissler, A., Wurnig, M.C., Matt, E., Rath, J., Robinson, S.D., Trattnig, S., Beisteiner, R., 2013. The benefits of skull stripping in the normalization of clinical fMRI data. Neuroimage Clin. 3, 369–380.

Frey, S., Pandya, D.N., Chakravarty, M.M., Bailey, L., Petrides, M., Collins, D.L., 2011. An MRI based average macaque monkey stereotaxic atlas and space (MNI monkey space). Neuroimage 55, 1435–1442.

Gorgolewski, K.J., Auer, T., Calhoun, V.D., Craddock, R.C., Das, S., Duff, E.P., Flandin, G., Ghosh, S.S., Glatard, T., Halchenko, Y.O., Handwerker, D.A., Hanke, M., Keator, D., Li, X., Michael, Z., Maumet, C., Nichols, B.N., Nichols, T.E., Pellman, J., Poline, J.B., Rokem, A., Schaefer, G., Sochat, V., Triplett, W., Turner, J.A., Varoquaux, G., Poldrack, R.A., 2016. The brain imaging data structure, a format for organizing and describing outputs of neuroimaging experiments. Sci. Data 3, 160044.

Hagberg, G.E., Bianciardi, M., Brainovich, V., Cassara, A.M., Maraviglia, B., 2008. The effect of physiological noise in phase functional magnetic resonance imaging: from blood oxygen level-dependent effects to direct detection of neuronal currents. Magn. Reson. Imaging 26, 1026–1040.

In, M.H., Cho, S., Shu, Y., Min, H.K., Bernstein, M.A., Speck, O., Lee, K.H., Jo, H.J., 2017. Correction of metal-induced susceptibility artifacts for functional MRI during deep brain stimulation. Neuroimage 158, 26–36.

Joly, O., Pallier, C., Ramus, F., Pressnitzer, D., Vanduffel, W., Orban, G.A., 2012a. Processing of vocalizations in humans and monkeys: a comparative fMRI study. Neuroimage 62, 1376–1389.

Joly, O., Ramus, F., Pressnitzer, D., Vanduffel, W., Orban, G.A., 2012b. Interhemispheric differences in auditory processing revealed by fMRI in awake rhesus monkeys. Cerebr. Cortex 22, 838–853.

Jones, Eric, Oliphant, Travis, Peterson, Pearu, 2001. SciPy: Open Source Scientific Tools for Python.

Kaas, J.H., Hackett, T.A., 2000. Subdivisions of auditory cortex and processing streams in primates. Proc. Natl. Acad. Sci. U. S. A. 97, 11793–11799.

Keliris, G.A., Shmuel, A., Ku, S.P., Pfeuffer, J., Oeltermann, A., Steudel, T., Logothetis, N.K., 2007. Robust controlled functional MRI in alert monkeys at high magnetic field: effects of jaw and body movements. Neuroimage 36, 550–570.

Kraskov, A., Stogbauer, H., Grassberger, P., 2004. Estimating mutual information. Phys. Rev. E - Stat. Nonlinear Soft Matter Phys. 69, 066138.

Leite, F.P., Tsao, D., Vanduffel, W., Fize, D., Sasaki, Y., Wald, L.L., Dale, A.M., Kwong, K.K., Orban, G.A., Rosen, B.R., Tootell, R.B., Mandeville, J.B., 2002. Repeated fMRI using iron oxide contrast agent in awake, behaving macaques at 3 Tesla. Neuroimage 16, 283–294.

Logothetis, N.K., Guggenberger, H., Peled, S., Pauls, J., 1999. Functional imaging of the monkey brain. Nat. Neurosci. 2, 555–562.

Logothetis, N.K., Pauls, J., Augath, M., Trinath, T., Oeltermann, A., 2001. Neurophysiological investigation of the basis of the fMRI signal. Nature 412, 150–157.

Marques, J.P., Kober, T., Krueger, G., van der Zwaag, W., Van de Moortele, P.F., Gruetter, R., 2010. MP2RAGE, a self bias-field corrected sequence for improved segmentation and T1-mapping at high field. Neuroimage 49, 1271–1281.

Mikl, M., Marecek, R., Hlustik, P., Pavlicova, M., Drastich, A., Chlebus, P., Brazdil, M., Krupa, P., 2008. Effects of spatial smoothing on fMRI group inferences. Magn. Reson. Imaging 26, 490–503.

Milham, M.P., Ai, L., Koo, B., Xu, T., Amiez, C., Balezeau, F., Baxter, M.G., Blezer, E.L.A., Brochier, T., Chen, A., Croxson, P.L., Damatac, C.G., Dehaene, S., Everling, S., Fair, D.A., Fleysher, L., Freiwald, W., Froudist-Walsh, S., Griffiths, T.D., Guedj, C., Hadj-Bouziane, F., Ben Hamed, S., Harel, N., Hiba, B., Jarraya, B., Jung, B., Kastner, S., Klink, P.C., Kwok, S.C., Laland, K.N., Leopold, D.A., Lindenfors, P., Mars, R.B., Menon, R.S., Messinger, A., Meunier, M., Mok, K., Morrison, J.H., Nacef, J., Nagy, J., Rios, M.O., Petkov, C.I., Pinsk, M., Poirier, C., Procyk, E., Rajimehr, R., Reader, S.M., Roelfsema, P.R., Rudko, D.A., Rushworth, M.F.S., Russ, B.E., Sallet, J., Schmid, M.C., Schwiedrzik, C.M., Seidlitz, J., Sein, J., Shmuel, A., Sullivan, E.L., Ungerleider, L., Thiele, A., Todorov, O.S., Tsao, D., Wang, Z., Wilson, C.R.E., Yacoub, E., Ye, F.Q., Zarco, W., Zhou, Y.D., Margulies, D.S., Schroeder, C.E., 2018. An open resource for non-human primate imaging. Neuron 100, 61–74 e2.

Min, H.K., Ross, E.K., Lee, K.H., Dennis, K., Han, S.R., Jeong, J.H., Marsh, M.P., Striemer, B., Felmlee, J.P., Lujan, J.L., Goerss, S., Duffy, P.S., Blaha, C., Chang, S.Y., Bennet, K.E., 2014. Subthalamic nucleus deep brain stimulation induces motor network BOLD activation: use of a high precision MRI guided stereotactic system for nonhuman primates. Brain Stimul. 7, 603–607.

Murphy, K., Birn, R.M., Bandettini, P.A., 2013. Resting-state fMRI confounds and cleanup. Neuroimage 80, 349–359.

Orban, G.A., Fize, D., Peuskens, H., Denys, K., Nelissen, K., Sunaert, S., Todd, J., Vanduffel, W., 2003. Similarities and differences in motion processing between the human and macaque brain: evidence from fMRI. Neuropsychologia 41, 1757–1768.

Orban, G.A., Van Essen, D., Vanduffel, W., 2004. Comparative mapping of higher visual areas in monkeys and humans. Trends Cogn. Sci. 8, 315–324.

Ortiz-Rios, M., Kusmierek, P., DeWitt, I., Archakov, D., Azevedo, F.A., Sams, M., Jaaskelainen, I.P., Keliris, G.A., Rauschecker, J.P., 2015. Functional MRI of the vocalization-processing network in the macaque brain. Front. Neurosci. 9, 113.

Petkov, C.I., Kayser, C., Augath, M., Logothetis, N.K., 2006. Functional imaging reveals numerous fields in the monkey auditory cortex. PLoS Biol. 4, e215.

Pfeuffer, J., Shmuel, A., Keliris, G.A., Steudel, T., Merkle, H., Logothetis, N.K., 2007. Functional MR imaging in the awake monkey: effects of motion on dynamic off-resonance and processing strategies. Magn. Reson. Imaging 25, 869–882.

Reveley, C., Gruslys, A., Ye, F.Q., Glen, D., Samaha, J., Russ B, E., Saad, Z., Seth A, K., Leopold, D.A., Saleem, K.S., 2017. Three-dimensional digital template Atlas of the macaque brain. Cerebr. Cortex 27, 4463–4477.

Rohlfing, T., Kroenke, C.D., Sullivan, E.V., Dubach, M.F., Bowden, D.M., Grant, K.A., Pfefferbaum, A., 2012. The INIA19 template and NeuroMaps atlas for primate brain image parcellation and spatial normalization. Front. Neuroinf. 6, 27.

Saenger, V.M., Kahan, J., Foltynie, T., Friston, K., Aziz, T.Z., Green, A.L., van Hartevelt, T.J., Cabral, J., Stevner, A.B.A., Fernandes, H.M., Mancini, L., Thornton, J., Yousry, T., Limousin, P., Zrinzo, L., Hariz, M., Marques, P., Sousa, N., Kringelbach, M.L., Deco, G., 2017. Uncovering the underlying mechanisms and

whole-brain dynamics of deep brain stimulation for Parkinson's disease. Sci. Rep. 7, 9882.
Scouten, A., Papademetris, X., Constable, R.T., 2006. Spatial resolution, signal-to-noise ratio, and smoothing in multi-subject functional MRI studies. Neuroimage 30, 787–793.
Seidlitz, J., Sponheim, C., Glen, D., Ye, F.Q., Saleem, K.S., Leopold, D.A., Ungerleider, L., Messinger, A., 2018. A population MRI brain template and analysis tools for the macaque. Neuroimage 170, 121–131.
Shmuel, A., Leopold, D.A., 2008. Neuronal correlates of spontaneous fluctuations in fMRI signals in monkey visual cortex: implications for functional connectivity at rest. Hum. Brain Mapp. 29 (7), 751–761.
Smith, S.M., Jenkinson, M., Woolrich, M.W., Beckmann, C.F., Behrens, T.E., Johansen-Berg, H., Bannister, P.R., De Luca, M., Drobnjak, I., Flitney, D.E., Niazy, R.K., Saunders, J., Vickers, J., Zhang, Y., De Stefano, N., Brady, J.M., Matthews, P.M., 2004. Advances in functional and structural MR image analysis and implementation as FSL. Neuroimage 1 (23 Suppl), S208–S219.
Tolias, A.S., Sultan, F., Augath, M., Oeltermann, A., Tehovnik, E.J., Schiller, P.H., Logothetis, N.K., 2005. Mapping cortical activity elicited with electrical microstimulation using FMRI in the macaque. Neuron 48, 901–911.
Uhrig, L., Dehaene, S., Jarraya, B., 2014. A hierarchy of responses to auditory regularities in the macaque brain. J. Neurosci. 34, 1127–1132.
Uhrig, L., Janssen, D., Dehaene, S., Jarraya, B., 2016. Cerebral responses to local and global auditory novelty under general anesthesia. Neuroimage 141, 326–340.
Uhrig, L., Sitt, J.D., Jacob, A., Tasserie, J., Barttfeld, P., Dupont, M., Dehaene, S., Jarraya, B., 2018. Resting-state dynamics as a cortical signature of anesthesia in monkeys. Anesthesiology 129, 942–958.
Valette, J., Guillermier, M., Boumezbeur, F., Poupon, C., Amadon, A., Hantraye, P., Lebon, V., 2006. B(0) homogeneity throughout the monkey brain is strongly improved in the sphinx position as compared to the supine position. J. Magn. Reson. Imaging 23, 408–412.
Vanduffel, W., Fize, D., Mandeville, J.B., Nelissen, K., Van Hecke, P., Rosen, B.R., Tootell, R.B., Orban, G.A., 2001. Visual motion processing investigated using contrast agent-enhanced fMRI in awake behaving monkeys. Neuron 32, 565–577.
Wang, L., Uhrig, L., Jarraya, B., Dehaene, S., 2015. Representation of numerical and sequential patterns in macaque and human brains. Curr. Biol. 25, 1966–1974.
Yoo, T.S., Ackerman, M.J., Lorensen, W.E., Schroeder, W., Chalana, V., Aylward, S., Metaxas, D., Whitaker, R., 2002. Engineering and algorithm design for an image processing Api: a technical report on ITK–the Insight Toolkit. Stud. Health Technol. Inform. 85, 586–592.